



## PAPER

[View Article Online](#)  
[View Journal](#) | [View Issue](#)Cite this: *Dalton Trans.*, 2025, **54**,  
5747Functionalized organotellurium macrocycles:  
tuning their optical bandgap and investigation of  
their catalytic activity†Calvin Samuel,<sup>a</sup> Velpula Pramod,<sup>a</sup> Swandhana V. S.,<sup>a</sup> Alexander Steiner <sup>\*b</sup> and  
Viswanathan Baskar <sup>\*a</sup>

This work deals with the synthesis, characterization, and optical properties of 12-membered tellurium macrocycles functionalized with an allyl group. These are synthesized by the reaction of bis-*p*-methoxyphenyl tellurium dihalide with phenyl allyl phosphinic acid at room temperature. SCXRD reveals that the cationic macrocycle is capped by two halide ions giving an overall composition of  $[(p\text{-OMePh})_2\text{Te}]_2(\text{O})(\text{PhC}_3\text{H}_5\text{PO}_2)(\mu_4\text{-X})_2$ , where X = Cl (Cl-TAM) and Br (Br-TAM). On reacting Cl-TAM with KI, we were able to isolate the iodo-capped macrocycle  $[(p\text{-OMePh})_2\text{Te}]_2(\text{O})(\text{PhC}_3\text{H}_5\text{PO}_2)(\mu_4\text{-I})_2$  (I-TAM). The presence of allyl groups at the periphery would allow these macrocycles to act as potential building blocks. Optical absorption studies show that the bandgap can be tuned by exchanging the capping halides. These systems were also found to act as catalysts for the detoxification of CEES, a mustard gas simulant.

Received 5th December 2024,  
Accepted 6th March 2025  
DOI: 10.1039/d4dt03388d[rsc.li/dalton](http://rsc.li/dalton)

## Introduction

Over previous decades, macrocycles have been a focal subject in both synthetic and materials chemistry due to their numerous applications in host–guest chemistry,<sup>1–7</sup> gas storage,<sup>8</sup> and the modeling of biological systems,<sup>9</sup> and as anion trapping devices for improving conductivity.<sup>10</sup> In recent decades, the interest in organotellurium(II/IV) based chemistry has been steadily growing.<sup>11</sup> These systems have the potential to trap anions using secondary interactions which were first demonstrated by Beckmann *et al.* by treating organotellurium with organotin under an atmosphere of CO<sub>2</sub> at room temperature.<sup>12,13</sup> Diorganotellurium/oxide/halides have the ability to form macrocycles<sup>14–17</sup> with various protic acids<sup>18–23</sup> resulting in the isolation of new telluroxane frameworks. Recently, 2D and 3D covalent organic polymers have been assembled *via* Te–O–P linkages.<sup>24</sup> Telluronium ions have also been found to act as active sites for Lewis acid receptors which work as catalysts.<sup>25</sup> The same group has also explored the oxidative alkylation of diaryl tellurides  $[\text{Mes}(\text{C}_6\text{F}_5)_2\text{TeMe}]^+$  and  $[(\text{C}_6\text{F}_5)_2\text{TeMe}]^+$  from  $\text{Mes}(\text{C}_6\text{F}_5)_2\text{Te}$  and  $(\text{C}_6\text{F}_5)_2\text{Te}$ , respectively.<sup>26</sup> These telluronium salts can form complexes and transport

chloride ions across phospholipid bilayers, thus finding application in ion transport. Also, the catalytic properties of a tetrafluoroborate salt of bis-telluronium dications have been studied.<sup>27</sup> Many research groups have diligently utilized organotellurium(II) compounds as catalysts,<sup>28–30</sup> while organotellurium systems in the +IV oxidation state remain less explored. Our research group synthesized analogs of 12-membered organotellurium(IV) macrocycles functioning as building blocks for organometallic–inorganic hybrid materials, which were found to act as electrocatalysts for the reduction of nitrate to ammonia.<sup>31</sup> Also, we have utilized weak anions like BF<sub>4</sub><sup>−</sup> and ClO<sub>4</sub><sup>−</sup> as bridging ligands to assemble organotellurium(IV) macrocycles, wherein the BF<sub>4</sub><sup>−</sup> analogue has shown to act as an electrocatalyst for the hydrogen evolution reaction (HER).<sup>32</sup>

Previously, we have explored the reactivity of diorganotellurium dihalides with benzene seleninic acid, resulting in 12-membered macrocycles  $[(p\text{-MeO-C}_6\text{H}_4)_2\text{Te}(\mu\text{-O})(\mu\text{-PhSeO}_2)(\mu_4\text{-X})_2]$  [X = Cl, Br, and I] where the halide ions, stabilized by Te...X interactions, cap the dicationic macrocycles on both sides.<sup>33</sup> Furthermore, we have exchanged the chloride anion with anions of varying geometries like trigonal planar (NO<sub>3</sub><sup>−</sup>) and tetrahedral (ClO<sub>4</sub><sup>−</sup>, BF<sub>4</sub><sup>−</sup>) by reacting the chloro-macrocycle  $[(p\text{-MeO-C}_6\text{H}_4)_2\text{Te}(\mu\text{-O})(\mu\text{-PhSeO}_2)(\mu_4\text{-Cl})_2]$  with AgNO<sub>3</sub>, AgClO<sub>4</sub>, and AgBF<sub>4</sub>.<sup>34</sup> Recently, we have synthesized heterometallic systems wherein the change in the metal ion influences the optical bandgap.<sup>35,36</sup> In this work, we present three isostructural, 12-membered tellurium macrocycles capped with different halides of the formula  $[(p\text{-MeO-C}_6\text{H}_4)_2\text{Te}(\mu\text{-O})(\mu\text{-PhC}_3\text{H}_5\text{PO}_2)(\mu_4\text{-X})_2]$ , where X = Cl, Br, or I. The Chloro-capped Tellurium Allyl Macrocycle (Cl-TAM) and the Bromo-capped Tellurium Allyl

<sup>a</sup>School of Chemistry, University of Hyderabad, Hyderabad – 500046, India.E-mail: [vbasc@uohyd.ac.in](mailto:vbasc@uohyd.ac.in)<sup>b</sup>Department of Chemistry, University of Liverpool, Crown Street, Liverpool L69 7ZD, UK†Electronic supplementary information (ESI) available. CCDC 2407188 and 2407189. For ESI and crystallographic data in CIF or other electronic format see DOI: <https://doi.org/10.1039/d4dt03388d>

Macrocycle (Br-TAM) were prepared by reacting the diorganotellurium halide with phenyl allyl phosphinic acid while the Iodo-capped Tellurium Allyl Macrocycle (I-TAM) was synthesized by reacting Cl-TAM with NaI in acetone. We have investigated the change in optical bandgaps by varying the halides. Moreover, the catalytic scope of these systems for detoxifying a mustard gas simulant under mild oxidizing conditions has been investigated.

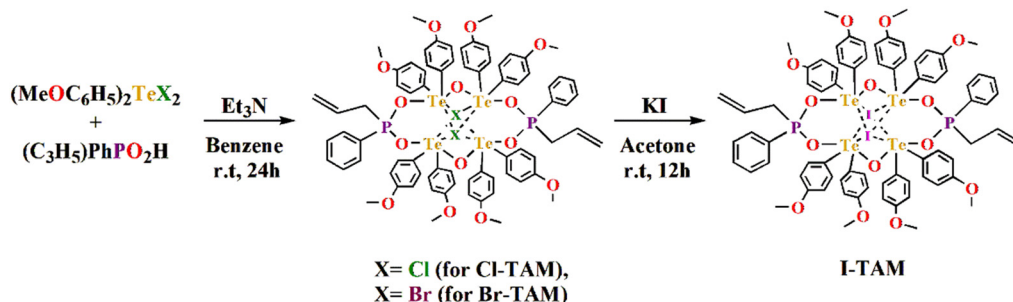
## Results and discussion

Cl-TAM and Br-TAM were synthesized by reacting phenyl allyl phosphinic acid with  $R_2TeX_2$  [ $R = p$ -methoxyphenyl,  $X = Cl$  (for Cl-TAM) and  $Br$  (for Br-TAM)] in benzene at room temperature using triethylamine as a base (Scheme 1). The formation of an oxo-bridge in the ditelluroxane moiety might have probably arisen from adventitious water present in the solvent. I-TAM was synthesized by reacting Cl-TAM with KI in acetone, which led to a simple halide exchange. Colourless crystals of Cl-TAM were obtained by slow evaporation of the mother liquor, while crystals of Br-TAM were grown from a benzene/chloroform mixture. The diffusion of hexane to benzene solution yielded yellow colour crystals of I-TAM. Spectroscopic and analytical data of Cl-TAM were reported in previous work in which the macrocycle was used as a building block for hybrid materials.<sup>31</sup> The IR spectra of Br-TAM and I-TAM show characteristic P–O–M stretching frequencies at  $1059\text{ cm}^{-1}$  and  $1060\text{ cm}^{-1}$  (Fig. S1 and S2†). The  $^1H$  NMR spectrum of Br-TAM exhibits two peaks at  $\delta$  4.5 ppm and  $\delta$  4.7 ppm, while a multiplet was observed at  $\delta$  5.5 ppm (Fig. S3†). Similarly, for I-TAM, two peaks and a multiplet were observed at  $\delta$  4.8 ppm, 4.9 ppm, and 5.5 ppm, respectively (Fig. S4†). These peaks, though of low intensity due to low abundance of allylic hydrogens, are distinct, thereby confirming the presence of allyl groups in both these compounds. The  $^{31}P\{^1H\}$  NMR spectrum of Br-TAM exhibits a singlet at  $\delta$  26.9 ppm, while that of I-TAM shows a peak at  $\delta$  29.1 ppm (Fig. S5 and S6†). The ESI-MS spectra of Br-TAM and I-TAM show  $m/z$  peaks at 1828.8461 (Fig. S7†) and 1888.9815 (Fig. S8†) which correspond to  $[(p\text{-OMeC}_6\text{H}_4)_2\text{Te}_2\text{O}(\text{Ph}(\text{C}_3\text{H}_5)\text{PO}_2)_2\{X\}]^+$  formed by the loss of one halide ion. The phase purity of crystalline Br-TAM and I-TAM was confirmed using PXRD, which correlates well with

the simulated pattern obtained from SCXRD data (Fig. S9 and S10†). The thermal stability of the systems was analysed using TGA which showed that Br-TAM and I-TAM were fairly stable up to  $250^\circ\text{C}$ , after which they decomposed (Fig. S11 and S12†). The elemental mapping corroborated the presence of  $Br$  and  $I$  in these systems (Fig. S15 and S18†).

Br-TAM crystallizes in the space group  $P2_1/n$ , while I-TAM crystallizes in  $P\bar{1}$ . The asymmetric unit of Br-TAM contains half a macrocycle while I-TAM contains two half macrocycles. The crystallographic information can be found in Table S1.† Br-TAM and I-TAM are isostructural with just a change in the capping halide; Br-TAM will be taken as the representative structure for structural description. Br-TAM comprises two ditelluroxane units bridged by a phosphinate on either side with a bromide ion above and below the macrocycle (Fig. 1). The macrocycle core is dicationic, and the bromides are held by secondary interactions, balancing the charge. The 12-membered macrocycle is nearly planar. The tetravalent  $Te$  atoms show the characteristic disphenoidal geometry with  $O\text{--}Te\text{--}O$  angles of  $168.68(16)^\circ$  at  $Te1$  and  $169.24(16)^\circ$  at  $Te2$ , while the  $C\text{--}Te\text{--}C$  angles are  $97.4(2)^\circ$  at  $Te1$  and  $96.9(2)^\circ$  at  $Te2$ . The angle at the  $O$ -atom bridging the two  $Te$  atoms measures  $125.1(2)^\circ$  with  $Te\text{--}O$  distances of  $1.972(4)\text{ \AA}$  to  $Te1$  and  $1.983(4)\text{ \AA}$  to  $Te2$ . The  $Te\text{--}O$  distances to the phosphinate units are somewhat longer, measuring  $2.368(4)\text{ \AA}$  for  $Te1\text{--}O2$  and  $2.353(4)\text{ \AA}$  for  $Te2\text{--}O3$ . The phosphinates carry phenyl and allyl groups at the periphery of the macrocycle. As demonstrated in our previous work, functionalization with allyl groups could facilitate the generation of extended systems for hybrid materials.<sup>31</sup> The bromide is held by a secondary interaction with  $Te$  and has a distance to  $Te1$  and  $Te2$  of  $3.543\text{ \AA}$  and  $3.357\text{ \AA}$ , respectively. Overall, the structure resembles a reverse-crown ether, where the macrocycle has a cationic core instead of an anionic core.

Tuning of the optical bandgap has great implications in the field of optoelectronics. Over the years, various strategies have been employed to produce molecular structures and materials with varying bandgaps.<sup>37–40</sup> It was observed that the bandgap of perovskites could be tuned by simple halide exchange.<sup>41–43</sup> We wanted to investigate if the optical bandgap can be tuned by changing the halide capping. The solid-state UV-visible absorption spectra were recorded for compounds Cl-TAM, Br-TAM, and I-TAM (Fig. S20–S22†). The optical bandgaps for



Scheme 1 Synthesis of macrocycles.

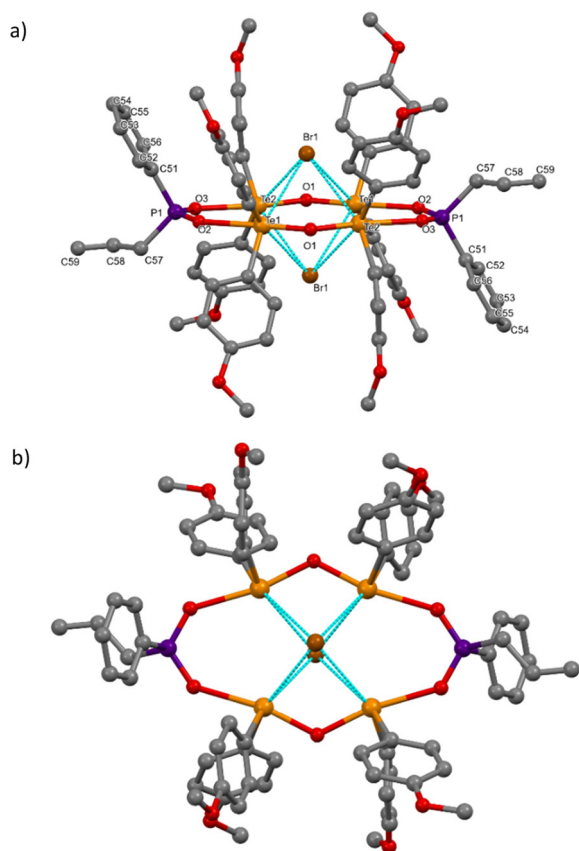


**Fig. 1** (a) Molecular structure of Br-TAM. (b) Top view. Color code: orange – Te, brown – I, purple – P, red – O, and grey – C. Hydrogens and the chloroform solvate are omitted for clarity.

these chloro-capped, bromo-capped and iodo-capped macrocycles were calculated using the Tauc equation.

$$(\alpha h\nu)^{1/n} = A(h\nu - E_g)$$

where  $h\nu$  is the photon energy,  $\alpha$  is the absorption coefficient,  $E_g$  is the bandgap energy, and  $A$  is a constant.  $n$  represents the type of electron transition and its value is  $\frac{1}{2}$  for a direct bandgap and 2 for an indirect bandgap. We calculated the direct bandgap, so the graph was plotted between  $(\alpha h\nu)^2$  and  $h\nu$ . The  $E_g$  value was calculated using the linear fit of the fundamental peak. Additionally, a linear fit used as an abscissa is applied for the slope below the fundamental absorption. An intersection of the two fitting lines gives the bandgap energy estimation.<sup>44</sup> Using this method, a bandgap of 3.17 eV was observed for Cl-TAM (Fig. 2a), while for Br-TAM, a slightly lower bandgap of 3.09 eV was observed (Fig. 2b). Finally, for I-TAM a bandgap of 2.25 eV was detected (Fig. 2c), showing that the bandgap could be tuned in these tellurium macrocycles by simple halide exchange. As stated before, this kind of tuning achieved through halide exchange is witnessed in inorganic lead perovskite systems but it has to be noted that the nature of Te–X bonds in the macrocycles is quite different from the bonds seen in perovskites. The halides are held to

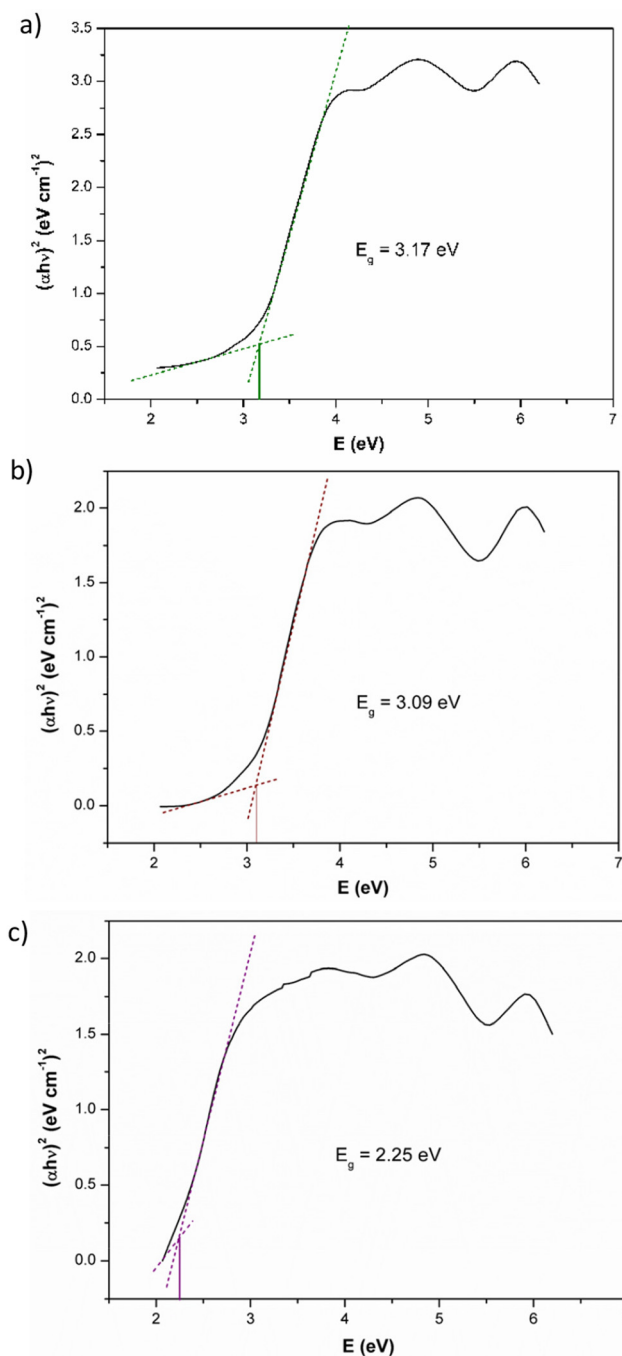


**Fig. 2** Tauc plots of (a) Cl-TAM, (b) Br-TAM, and (c) I-TAM.

the tellurium by weak secondary interactions, so as we move towards bigger anions, the interactions become stronger, which results in a smaller HOMO–LUMO gap.

Furthermore, the catalytic activity of the diorganotellurium macrocycle was investigated. The oxidation of 2-chloroethyl ethyl sulfide (CEES), an organosulfide compound that is a chemical simulant for the toxic chemical warfare agent, mustard gas, is performed. It is important to selectively oxidize it to the non-toxic 2-chloroethyl ethyl sulfoxide (CEESO) but not to 2-chloroethyl ethyl sulfone (CEESO<sub>2</sub>).<sup>45–50</sup>

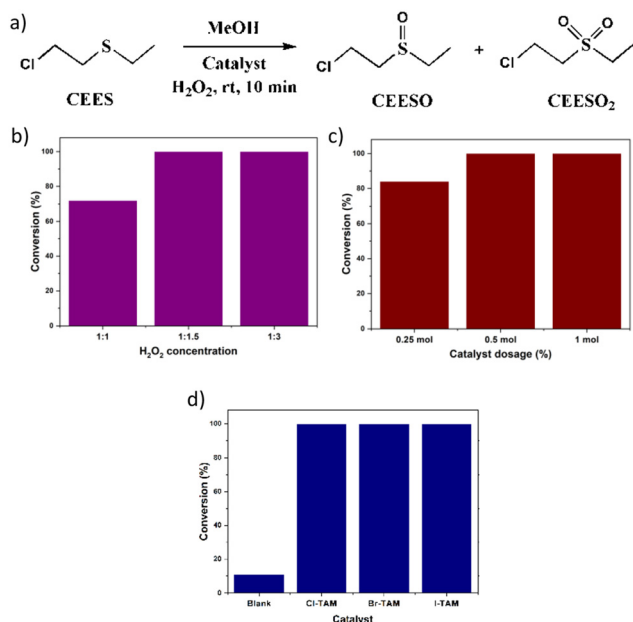


**Fig. 3** (a) Scheme for the oxidation of CEES, (b) H<sub>2</sub>O<sub>2</sub> concentration vs. conversion plot, (c) catalyst dosage vs. conversion plot and (d) catalysts vs. conversion plot.

Knowing the potential of the telluroxane system to act as a catalyst, we decided to evaluate its ability to detoxify CEES. First, the reaction was optimized using Cl-TAM. Under homogeneous conditions, using methanol as a solvent and H<sub>2</sub>O<sub>2</sub> as an oxidant at room temperature, a good conversion was established. After varying the H<sub>2</sub>O<sub>2</sub> concentration, 1.5 eq. was found to give complete conversion with 100% selectivity to CEESO (Fig. 3b). The catalyst dosage was also varied with 0.5 mol% and 1 mol% giving 100% conversion (Fig. 3c). 0.5 mol% was applied as the optimum dosage. In the same manner, Br-TAM and I-TAM were evaluated and they showed similar activity with 100% conversion and 100% selectivity to CEESO (Fig. 3d). This shows that the change in halide capping does not visibly influence the catalytic activity. The same reaction in the absence of the catalysts showed only 11% conversion. After the reaction, the solvent was removed and Cl-TAM was separated, washed, and dried. The IR spectra of Cl-TAM matched the IR spectra taken before catalysis, proving that the catalyst was stable (Fig. S23†). Finally, to deduce the mechanism, the reaction was performed in the presence of TEMPO, but no change in the conversion was observed. This ruled out the possibility of radical formation. So, based on that, it was concluded that the reaction plausibly proceeds *via* the peroxidase pathway (Fig. S24†). Initially, the tellurium active site interacts with H<sub>2</sub>O<sub>2</sub> to form Te-OOH species.<sup>51,52</sup> This, in turn, oxidizes CEES to CEESO, and the catalyst is regenerated.

## Conclusions

In summary, we present three isostructural 12-membered tellurium macrocycles capped with different halides, Cl-TAM, Br-

TAM, and I-TAM. We further investigated the effect of halide exchange on the optical bandgap and found that the bandgap decreases in the order Cl to Br to I. The iodo-capped macrocycle shows the lowest bandgap, probably due to the size of the anion. This approach can potentially generate hybrid materials with a wide range of bandgap energies which will have interesting applications in the field of optoelectronics. We also utilized these systems as catalysts for the detoxification of CEES, a mustard gas simulant. All three macrocycles showed excellent conversion with high selectivity.

## Experimental section

### General information

Phenyl allyl phosphinic acid<sup>53</sup> and bis(*p*-methoxyphenyl) tellurium dichloride<sup>54</sup> were synthesized according to literature reports. Phenyl phosphinic acid and TeCl<sub>4</sub> were purchased from Sigma-Aldrich, benzene and acetone were purchased from Finar, and allyl bromide, KI, and anisole were purchased from Avra. All solvents and reagents were purified before use by adopting standard methods.

### Instrumentation

Infrared spectra were recorded using a Nicolet iS5 FTIR spectrometer. ESI-MS spectra were recorded using Bruker MaXis HRMS (ESI-TOF analyzer) equipment. NMR spectra were recorded using Bruker Avance-400 and 500 MHz FT NMR spectrometers at room temperature. Single crystal X-ray diffraction (SCXRD) data collection for Br-TAM and I-TAM was carried out at room temperature with an XtaLAB Synergy, a single source at offset/far, HyPix3000 diffractometer, and a Rigaku Oxford HyPix3000 CCD plate detector system [ $\lambda(\text{Mo K}\alpha) = 0.71073 \text{ \AA}$ ] with a mirror monochromator. The data were reduced using CrysAlisPro 1.171.40.35a (Rigaku OD, 2018). The structures were solved using SHELXT and refined using SHELXL-2018/3 in Olex2 1.3-ac4 software.<sup>55–57</sup> All non-hydrogen atoms were refined anisotropically except for disordered phenyl and allyl groups in I-TAM. Powder X-ray diffraction patterns were collected over the  $2\theta$  range of 5–50° at a scan rate of 3.9° min<sup>−1</sup>. TGA was recorded with a PerkinElmer STA 8000 thermogravimetric analyzer at a nitrogen gas flow rate of 20 ml min<sup>−1</sup> and a heating rate of 10 °C min<sup>−1</sup>. Field Emission-Scanning Electron Microscopy (FE-SEM) imaging, energy-dispersive spectroscopy (EDS) and elemental mapping were studied using an Ultra 55 Carl Zeiss instrument. Solid-state UV-vis absorption spectra were recorded with a JASCO-V-770 spectrophotometer. GC-MS was recorded with a Shimadzu GCMS-QP2020 NX. Graphics of the crystal structures have been generated using Mercury.

### General synthetic procedures

In a 50 mL round bottom flask, phenyl allyl phosphinic acid was dissolved in 10 mL of benzene, followed by the addition of triethylamine. After stirring for 5 minutes, bis(*p*-methoxyphenyl) tellurium dihalide was added, and the mixture was stirred



at room temperature for 24 hours. Afterward, the mixture was filtered, and crystals of Br-TAM were grown in a benzene/chloroform mixture. The isolated crystals were powdered and subjected to a high vacuum for 1 hour before being analyzed by standard spectroscopic and analytical techniques.

**Compound Br-TAM.** Phenyl allyl phosphinic acid (0.04 g, 0.2242 mmol), bis(*p*-methoxyphenyl) tellurium dibromide (0.22 g, 0.4485 mmol), and triethylamine (0.07 mL, 0.4932 mmol) were used. Yield: 0.15 g (70%). Formula: C<sub>74</sub>H<sub>76</sub>Br<sub>2</sub>O<sub>14</sub>P<sub>2</sub>Te<sub>4</sub>. ESI-MS: 1828.8461 for [M-CH<sub>2</sub>Br]<sup>+</sup>. <sup>1</sup>H NMR (500 MHz, DMSO-d<sub>6</sub>, ppm): δ 7.9–6.8 (m), δ 5.5 (m), δ 4.7 (d), δ 4.5 (d), δ 3.7 (s). <sup>31</sup>P{<sup>1</sup>H} NMR (158 MHz, DMSO-d<sub>6</sub>, ppm): δ 27.7 (s). IR: 3049.96 (w), 3005.47 (w), 2989.59 (w), 2836.49 (w), 1582.18 (s), 1488.89 (s), 1456.35 (s), 1437.63 (s), 1399.70 (m), 1291.54 (s), 1246.50 (s), 1173.65 (s), 1113.27 (s), 1059.93 (m), 1004.90 (s), 915.83 (m), 820.22 (s), 787.23 (s), 749.91 (m), 715.10 (m), 658.69 (s), 609.70 (m), 568.26 (m), 553.20 (s), 509.55 (s).

The general synthetic procedure for I-TAM is that in a 50 mL round bottom flask, Cl-TAM was dissolved in 15 mL of acetone, followed by the addition of KI. The mixture was stirred at room temperature for 12 hours and filtered, and the solvent was removed *in vacuo*. The crystals of I-TAM were isolated from benzene by diffusing hexane. The isolated crystals were powdered and subjected to a high vacuum for 1 hour before being analyzed by standard spectroscopic and analytical techniques.

**Compound I-TAM.** Cl-TAM (0.100 g, 0.054 mmol) and KI (0.018 g, 0.109 mmol) were used. Yield: 0.05 g (90%). Formula: C<sub>74</sub>H<sub>76</sub>I<sub>2</sub>O<sub>14</sub>P<sub>2</sub>Te<sub>4</sub>. ESI-MS: 1888.9815 for [M – I]<sup>+</sup>. <sup>1</sup>H NMR (500 MHz, DMSO-d<sub>6</sub>, ppm): δ 7.7–6.9 (m), 5.5 (m), 4.9 (d), 4.8 (d), 3.7 (s). <sup>31</sup>P{<sup>1</sup>H} NMR (158 MHz, DMSO-d<sub>6</sub>, ppm): δ 29.1 (s). IR: 3065.84 (w), 3005.47 (w), 2935.07 (w), 2835.16 (w), 1582.31 (s), 1489.03 (s), 1457.42 (s), 1437.96 (s), 1398.71 (m), 1291.51 (s), 1246.78 (s), 1173.93 (s), 1111.81 (s), 1060.85 (m), 1005.21 (s), 917.20 (m), 820.46 (s), 786.87 (s), 747.34 (m), 698.09 (m), 664.87 (s), 611.97 (m), 590.21 (m).

### General procedure for the selective oxidation of CEES

In a typical experiment, CEES (1 mmol), H<sub>2</sub>O<sub>2</sub> (30 wt%, 1.5 mmol), and the catalyst (5 μmol) were added into a 50 mL round-bottom flask. The reaction mixture was charged at room temperature and stirred vigorously for a set time of 10 min. The resulting products were extracted with ethyl acetate, and analyzed by GC to determine the conversion and selectivity with mesitylene as an internal standard.

**Caution!** CEES is a valid simulant of HD and has a certain toxicity. Goggles, masks, and gloves are required for use, and the reaction should be carried out in a fume hood.

## Author contributions

C. S. conducted the investigation and formal analysis. V. P. and S. V. S. performed data validation. A. S. analyzed SCXRD data and reviewed the work. V. B. designed and conceptualized the research.

## Data availability

The ESI† has additional spectroscopic and analytical data. The crystal structures have been deposited at CCDC with deposition numbers 2407188 and 2407189.†

## Conflicts of interest

There are no conflicts to declare.

## Acknowledgements

We thank the SERB for funding (CRG/2023/000684).

## References

- 1 R. Gleiter, G. Haberhauer, D. B. Werz, F. Rominger and C. Bleiholder, *Chem. Rev.*, 2018, **118**, 2010–2041.
- 2 N. Biot, D. Romito and D. Bonifazi, *Cryst. Growth Des.*, 2021, **21**, 536–543.
- 3 N. Biot and D. Bonifazi, *Coord. Chem. Rev.*, 2020, **413**, 213243.
- 4 P. C. Ho, J. Lomax, V. Tomassetti, J. F. Britten and I. Vargas-Baca, *Chem. – Eur. J.*, 2021, **27**, 10849–10853.
- 5 P. C. Ho, P. Szydłowski, J. Sinclair, P. J. W. Elder, J. Kübel, C. Gendy, L. M. Lee, H. Jenkins, J. F. Britten, D. R. Morim and I. Vargas-Baca, *Nat. Commun.*, 2016, **7**, 11299.
- 6 G. Haberhauer and R. Gleiter, *Angew. Chem., Int. Ed.*, 2020, **59**, 21236–21243.
- 7 A. F. Cozzolino, P. J. W. Elder and I. Vargas-Baca, *Coord. Chem. Rev.*, 2011, **255**, 1426–1438.
- 8 H. Zhanga, R. Zoub and Y. Zhao, *Coord. Chem. Rev.*, 2015, **292**, 74–90.
- 9 O. Carugo, G. Resnati and P. Metrangolo, *ACS Chem. Biol.*, 2021, **16**, 1622–1627.
- 10 G. E. Garrett, E. I. Carrera, D. S. Seferos and M. S. Taylor, *Chem. Commun.*, 2016, **52**, 988.
- 11 S. Raju, H. B. Singh, S. Kumar and R. J. Butcher, *Chem. – Eur. J.*, 2023, **29**, e202301322.
- 12 J. Beckmann, D. Dakternieks, A. Duthie, N. A. Lewcenko and C. Mitchell, *Angew. Chem., Int. Ed.*, 2004, **43**, 6683–6685.
- 13 J. Beckmann, J. Bolsinger and A. Duthie, *Z. Anorg. Allg. Chem.*, 2010, **636**, 765–769.
- 14 K. Kobayashi, N. Deguchi, E. Horn and N. Furukawa, *Angew. Chem., Int. Ed.*, 1998, **37**, 984–986.
- 15 K. Kobayashi, N. Deguchi, O. Takahashi, K. Tanaka, E. Horn, O. Kikuchi and N. Furukawa, *Angew. Chem., Int. Ed.*, 1999, **38**, 1638–1640.
- 16 K. Kobayashi, H. Izawa, K. Yamaguchi, E. Horn and N. Furukawa, *Chem. Commun.*, 2001, 1428–1429.
- 17 J. Beckmann, D. Dakternieks, A. Duthie, N. A. Lewcenko, C. Mitchell and M. Schürmann, *Z. Anorg. Allg. Chem.*, 2005, **631**, 1856.

- 18 V. Chandrasekhar and R. Thirumoorthi, *Inorg. Chem.*, 2009, **48**, 10330.
- 19 R. K. Metre, S. Kundu, D. Sahoo and V. Chandrasekhar, *Organometallics*, 2014, **33**, 2380–2383.
- 20 N. W. Alcock, J. Culver and S. M. Roe, *J. Chem. Soc., Dalton Trans.*, 1992, 1477.
- 21 N. W. Alcock and W. D. Harrison, *J. Chem. Soc., Dalton Trans.*, 1982, 1421.
- 22 K. Kobayashi, H. Izawa, K. Yamaguchi, E. Hornc and N. Furukawaa, *Chem. Commun.*, 2001, 1428–1429.
- 23 J. Beckmann, J. Bolsinger and J. Spandl, *J. Organomet. Chem.*, 2008, **693**, 957–964.
- 24 M. Xue, L. Zhang, X.-X. Li, Z. Chen, F. Kang, X. Wang, Q. Dong, X. Wang, C.-S. Lee, Y.-Q. Lan and Q. Zhang, *Nat. Commun.*, 2024, **15**, 10026.
- 25 H. Zhu, P. P. Zhou and Y. Wang, *Nat. Commun.*, 2022, **13**, 3563.
- 26 B. Zhou and F. P. Gabbai, *Chem. Sci.*, 2020, **11**, 7495–7500.
- 27 B. Zhou and F. P. Gabbai, *J. Am. Chem. Soc.*, 2021, **143**, 8625–8630.
- 28 S. Jain, S. S. Satpute, R. K. Jha, M. S. Patel and S. Kumar, *Chem. – Eur. J.*, 2024, **30**, e202303089.
- 29 R. Weiss, E. Aubert, P. Pale and V. Mamane, *Angew. Chem., Int. Ed.*, 2021, **60**, 19281–19286.
- 30 S. Jain, M. Batabyal, R. A. Thorat, P. Choudhary, R. K. Jha and S. Kumar, *Chem. – Eur. J.*, 2023, **29**, e202301502.
- 31 C. Samuel, G. Narsimhulu, G. Bangar, S. H. K. Dasari, G. Rajaraman and V. Baskar, *Inorg. Chem.*, 2024, **63**, 21670–21678.
- 32 G. Narsimhulu, C. Samuel, S. Palani, S. H. K. Dasari, K. Krishnamoorthy and V. Baskar, *Dalton Trans.*, 2023, **52**, 17242–17248.
- 33 N. K. Srungavruksham and V. Baskar, *Eur. J. Inorg. Chem.*, 2012, 136–142.
- 34 N. K. Srungavruksham and V. Baskar, *Dalton Trans.*, 2015, **44**, 4554–4569.
- 35 U. Ugandhar, T. Navaneetha, J. Ali, S. Mondal, G. Vaitheeswaran and V. Baskar, *Inorg. Chem.*, 2020, **59**, 6689–6696.
- 36 T. Navaneetha, U. Ugandhar, C. Samuel, T. Guizouarn, F. Pointillart, R. Raghunathan and V. Baskar, *Dalton Trans.*, 2023, **52**, 9328–9336.
- 37 T. Shao, Y. Fang, C. He, L. Zhang and K. Wang, *Inorg. Chem.*, 2022, **61**, 5184–5189.
- 38 J.-X. Liu, M.-Y. Gao, W.-H. Fang, L. Zhang and J. Zhang, *Angew. Chem.*, 2016, **128**, 5246–5251.
- 39 C. K. Lin, D. Zhao, W. Y. Gao, Z. Yang, J. Ye, T. Xu, Q. Ge, S. Ma and D. J. Liu, *Inorg. Chem.*, 2012, **51**, 9039–9044.
- 40 A. Chanda, S. Gupta, M. Vasundhara, S. R. Joshi, G. R. Mutta and J. Singh, *RSC Adv.*, 2017, **7**, 50527–50536.
- 41 Y. Wu, P. Wang, Z. Guan, J. Liu, Z. Wang, Z. Zheng, S. Jin, Y. Dai, M.-H. Whangbo and B. Huang, *ACS Catal.*, 2018, **8**, 10349–10357.
- 42 D. M. Jang, K. Park, D. H. Kim, J. Park, F. Shojaei, H. S. Kang, J.-P. Ahn, J. W. Lee and J. K. Song, *Nano Lett.*, 2015, **15**, 5191–5199.
- 43 Q. A. Akkerman, V. D'Innocenzo, S. Accornero, A. Scarpellini, A. Petrozza, M. Prato and L. Manna, *J. Am. Chem. Soc.*, 2015, **137**, 10276–10281.
- 44 P. Makula, M. Pacia and W. Macyk, *J. Phys. Chem. Lett.*, 2018, **9**, 6814–6817.
- 45 X. Wang, K. Brunson, H. Xie, I. Colliard, M. C. Wasson, X. Gong, K. Ma, Y. Wu, F. A. Son, K. B. Idrees, X. Zhang, J. M. Notestein, M. Nyman and O. K. Farha, *J. Am. Chem. Soc.*, 2021, **143**, 21056–21065.
- 46 Q.-Y. Wang, Z.-B. Sun, M. Zhang, S.-N. Zhao, P. Luo, C.-H. Gong, W.-X. Liu and S.-Q. Zang, *J. Am. Chem. Soc.*, 2022, **144**, 21046–21055.
- 47 A. Atilgan, M. M. Cetin, J. Yu, Y. Beldjoudi, J. Liu, C. L. Stern, F. M. Cetin, T. Islamoglu, O. K. Farha, P. Deria, J. F. Stoddart and J. T. Hupp, *J. Am. Chem. Soc.*, 2020, **142**, 18554–18564.
- 48 V. Quezada-Novoa, H. M. Titi, A. A. Sarjeant and A. J. Howarth, *Chem. Mater.*, 2021, **33**, 4163–4169.
- 49 C. Lian, S.-H. Zhao, H.-L. Li and X. Cao, *Chin. Chem. Lett.*, 2023, 109343.
- 50 C. Samuel, T. Navaneetha, J. Ali and V. Baskar, *Inorg. Chem.*, 2025, **64**, 872–881.
- 51 E. E. Alberto, L. M. Muller and M. R. Detty, *Organometallics*, 2014, **33**, 5571–5581.
- 52 R. Kheirabadi and M. Izadyar, *Int. J. Quantum Chem.*, 2020, **120**, e26201.
- 53 E. A. Boyd, M. E. K. Boyd and V. M. Loh Jr., *Tetrahedron Lett.*, 1996, **37**, 1651–1654.
- 54 J. Bergman, *Tetrahedron*, 1972, **28**, 3323–3331.
- 55 O. V. Dolomanov, L. J. Bourhis, R. J. Gildea, J. A. K. Howard and H. J. Puschmann, *Appl. Crystallogr.*, 2009, **42**, 339–341.
- 56 G. M. Sheldrick, *Acta Crystallogr., Sect. A: Found. Adv.*, 2015, **71**, 3–8.
- 57 G. M. Sheldrick, *Acta Crystallogr., Sect. C: Struct. Chem.*, 2015, **71**, 3–8.